JOURNAL OF BACTERIOLOGY, Dec. 2004, p. 8326–8336 Vol. 186, No. 24
0021-9193/04/$08.00+0 DOI: 10.1128/JB.186.24.8326–8336.2004

Endopeptidase Penicillin-Binding Proteins 4 and 7 Play Auxiliary Roles in Determining Uniform Morphology of *Escherichia coli*

Bernadette M. Meberg, Avery L. Paulson,† Richa Priyadarshini, and Kevin D. Young*

Department of Microbiology and Immunology, University of North Dakota School of Medicine, Grand Forks, North Dakota

Received 29 July 2004/Accepted 8 September 2004

The low-molecular-weight (LMW) penicillin-binding protein, PBP 5, plays a dominant role in determining the uniform cell shape of *Escherichia coli*. However, the physiological functions of six other LMW PBPs are unknown, even though the existence and enzymatic activities of four of these were established three decades ago. By applying fluorescence-activated cell sorting (FACS) to quantify the cellular dimensions of multiple PBP mutants, we found that the endopeptidases PBP 4 and PBP 7 also influence cell shape in concert with PBP 5. This is the first reported biological function for these two proteins. In addition, the combined loss of three DD-carboxypeptidases, PBPs 5 and 6 and DacD, also impaired cell shape. In contrast to previous reports based on visual inspection alone, FACS analysis revealed aberrant morphology in a mutant lacking only PBP 5, a phenotype not shared by any other strain lacking a single LMW PBP. PBP 5 removes the terminal D-alanine from pentapeptide side chains of muropeptide subunits, and pentapeptides act as donors for cross-linking adjacent side chains. As endopeptidases, PBPs 4 and 7 cleave cross-links in the cell wall. Therefore, overall cell shape may be determined by the existence or location of a specific type of peptide cross-link, with PBP 5 activity influencing how many cross-links are made and PBPs 4 and 7 acting as editing enzymes to remove inappropriate cross-links.

Bacteria synthesize a rigid peptidoglycan exoskeleton for protection and to create and preserve a distinct cell shape. This sturdy outer wall counteracts a high internal osmotic pressure that would otherwise lyse cells growing in hypotonic environments, and several antibiotics exploit this vulnerability by interfering with peptidoglycan synthesis. The shape-defining role of the wall is less well appreciated, even though this characteristic is undoubtedly of important selective value. Cell shape influences motility (7), surface attachment (32), environmental dispersal (34), and susceptibility to predation (1) and may affect the course of microbial infection (8). However, in contrast to what we know about general peptidoglycan synthesis, we are only beginning to understand the mechanisms that generate specific bacterial shapes.

Current evidence indicates that cells employ two systems to generate shape. The first is governed by a group of cytoskeleton proteins, including FtsZ, MreB, and Mbl, which polymerize as filamentous rings or helices on the inner face of the cytoplasmic membrane (3, 9, 15). These apparently function as internal scaffolds that organize and direct the localization of proteins involved in cell division and elongation. The second system is composed of an array of periplasmic peptidoglycan-specific enzymes which polymerize, modify, degrade, and recycle peptidoglycan. Until recently, the proposal that the two systems interact has been not much more than an agreeable idea. However, Daniel and Errington bolstered this hypothesis by showing that an Mbl-dependent process inserts helical swaths of newly synthesized peptidoglycan into the cell wall of *Bacillus subtilis* (3). Also, Figge et al. observed that localization of an elongation-specific penicillin-binding protein (PBP) depends on the presence of MreB spirals within *Caulobacter crescentus* (9). Finally, the shape of *Escherichia coli* depends on a functional relationship between FtsZ and at least two low-molecular-weight (LMW) PBPs, such that SulA inhibition of FtsZ in a mutant lacking PBPs 5 and 7 produces spirillum-shaped cells (33). These observations imply that internal cytoplasmic fibers affect cell shape, possibly by positioning synthetic complexes so that they insert new peptidoglycan in a particular pattern around the cylindrical part of the wall. What determines the original size and shape of the cylinder is still a puzzle.

Previously, our group established that in *E. coli* PBP 5 plays a significant role in generating uniform cell shape via this second, extracytoplasmic system (23, 24). Mutants lacking PBP 5 and at least two additional LMW PBPs are markedly aberrant, in that such cells have unequal diameters and uneven contours and may be bent, kinked, blebbed, or branched (23). PBP 5 is of critical importance to this process, because as long as PBP 5 is active cell morphology is almost completely normal in mutants deficient in the other six LMW PBPs. Conversely, in the absence of PBP 5, no other LMW PBP restores normal cell shape (23, 24). Nonetheless, although PBP 5 is clearly essential to the phenotype, other PBPs must be involved, since prominent shape alterations are visible only in mutants lacking PBP 5 and at least two additional LMW PBPs (23).

We wished to identify more precisely the accessory PBPs responsible for morphological control in *E. coli*. A major limitation of previous experiments was that our assay was based entirely on microscopic evaluation, an approach that suffers from an inherent subjectivity because the observer's eye is drawn strongly to oddly shaped cells. In addition, the technique

* Corresponding author. Mailing address: Department of Microbiology and Immunology, University of North Dakota School of Medicine, Grand Forks, ND 58202-9037. Phone: (701) 777-2624. Fax: (701) 777-2054. E-mail: kyoung@medicine.nodak.edu.

† Present address: Department of Physiology and Life Sciences, Chadron State College, Chadron, NE 69337.

TABLE 1. *E. coli* strains

Strain	Genotype	PBP(s) deleted	Source or reference
KM-32	*argE3 his-4 leuB6 proA2 thr-1 ara-14 galK2 lacY1 mtl-1 xyl-5 thi-1 rpsL31 tsx-33 supE44* Δ(*recC ptr recB recD*)::P*lac-bet exo cmr*	None	21
BMKM16-1K	KM-32 *ybe-9207*::*res-npt-res* (Kan^r cassette insertion near *dacA*$^+$)	None	This work
KMAP-1K	KM-32 *yhbE-3650*::*res-npt-res* (Kan^r cassette insertion near *dacB*$^+$)	None	This work
KMAP-3K	KM-32 *yeh-7310*::*res-npt-res* (Kan^r cassette insertion near *pbpG*$^+$)	None	This work
CS109	W1485 *rpoS rph*	None	C. Schnaitman
BMCS16-1K	CS109 *ybe-9207*::*res-npt-res* (transduced from BMKM16-1K to CS109)	None	This work
APCS-1	CS109 *yhbE-3650*::*res-npt-res* (transduced from KMAP-1K to CS109)	None	This work
APCS-3	CS109 *yeh-7310*::*res-npt-res* (transduced from KMAP-3K to CS109)	None	This work
BMCS203-1K	CS109 Δ*dacB* Δ*pbpG ybe-9207*::*res-npt-res* (transduction of *dacA*$^+$ from BMCS16-1K to CS315-1)	4, 7	This work
APCS204-1K	CS109 Δ*dacA* Δ*pbpG yhbE-3650*::*res-npt-res* (transduction of *dacB*$^+$ from APCS-1 to CS315-1)	5, 7	This work
APCS219-1K	CS109 Δ*dacA* Δ*dacB yeh-7310*::*res-npt-res* (transduction of *pbpG*$^+$ from APCS-3 to CS315-1)	4, 5	This work

is insensitive in that slight deviations from normal morphology are difficult or impossible to detect and quantify, so that potential additive effects of multiple mutations may be overstated or go unrecognized. Therefore, to make these assessments more accurately, we quantified minor shape changes by using fluorescence-activated cell sorting (FACS). Using this approach, we identified PBPs 4 and 7 as auxiliary contributors to maintenance of normal rod shape in *E. coli*, which is the first specific biological role described for these proteins.

MATERIALS AND METHODS

Bacteria, plasmids, and growth conditions. Bacterial strains and plasmids are listed in Table 1 (see also Table 4, below). Bacteria were grown on Luria-Bertani (LB) broth or on LB agar plates (19). Bacteria to be evaluated by FACS were incubated in T-soy broth (Difco) from which interfering particulates had been removed by passage through a sterile 0.22-μm GP Express PLUS filter (Millipore, Billerica, Mass.). Strains containing pBAD18-Cm (from J. Beckwith) (11) or pBAD18-Cm-derived plasmids were grown in media supplemented with 20 μg of chloramphenicol/ml with or without 0.2% glucose, depending on whether cloned genes were to be repressed or expressed. Plasmid pBMM1 was constructed by excising the *res-npt-res* kanamycin resistance cassette from pCK155 (14) on a 2.1-kb EcoRI-HindIII DNA fragment and ligating it into the EcoRI-HindIII sites of pBCSK$^+$ (Cam^r Kan^r) (Stratagene, La Jolla, Calif.). Unless otherwise stated, chemicals were purchased from Sigma Chemical Co. (St. Louis, Mo.) or Fisher Scientific (Pittsburgh, Pa.).

General molecular techniques and PCR amplification. Plasmids were isolated by using QIAprep Spin Miniprep and Midiprep kits, and DNA was purified from agarose gels by using QIAquick gel extraction kits (QIAGEN Corp., Valencia, Calif.). Restriction enzymes were from New England Biolabs (Beverly, Mass.). Digestions, ligations, agarose electrophoresis, and preparation of electrocompetent cells were performed as described elsewhere (24, 29). Electrocompetent cells were transformed by utilizing the Gene Pulser (Bio-Rad Corp., Hercules, Calif.), according to the manufacturer's instructions.

Amplification by the PCR was performed in a model 2400 Gene Amp thermal cycler (Perkin-Elmer, Boston, Mass.). Chromosomal template from *E. coli* was prepared by boiling a mixture containing 3 parts overnight culture plus 7 parts distilled water for 10 min, as described previously (24). Primers for PCR were purchased from MWG Biotech (Highpoint, N.C.), and deoxynucleotide triphosphates were from Promega (Madison, Wis.). Deep Vent DNA polymerase was from New England Biolabs. Each PCR mixture contained a 200 nM concentration of each deoxynucleotide triphosphate, variable concentrations of primers (typically 200 pM), variable concentrations of template DNA, 2 U of Deep Vent DNA polymerase, 10 μl of 10× reaction buffer, and distilled water to bring the total volume to 100 μl. Reactions of 30 cycles were performed as follows: a 45-s denaturation step at 94°C, a 45-s annealing step at a temperature 4°C below the estimated melting temperature of the primer pair, and an extension step at 72°C for 1 min per kb of expected product. PCR products were purified by using the QIAquick PCR purification kit (QIAGEN Corp.).

Construction of chromosomal gene replacements. Wild-type PBP genes were linked to an antibiotic resistance marker so that the genes could be moved by P1 transduction to replace mutant alleles. For this purpose, a kanamycin resistance gene cassette was inserted near the chromosomal position of the wild-type genes for *dacA* (encoding PBP 5), *dacB* (encoding PBP 4), and *pbpG* (encoding PBP 7) (Fig. 1). The *res-npt-res* (kanamycin resistance) cassette from plasmid pBMM-1 was amplified by PCR utilizing the following primers: for insertion near the *dacA* gene, *dacA* forward (5′-TCAAAAATAGTCAGAAGGTTAAGATCAATATT TCGT-3′) and *dacA* reverse (5′-TTGGAGTAAGTGCGTGGATAGTAATAA TCAAATTGA-3′); for insertion near the *dacB* gene, *dacB* forward (5′-TGCC CCTACAACCTGAGTGCTGCGCATTTTCTCTTTGAGGAATTCGAGCTC TGCAGTCCC-3′) and *dacB* reverse (5′-TCATCCTTGCAATACCTGAGTCC GACCGCTTCGCAGGTGATAAGCTTGCATGCCTGCAG-3′); and for insertion near the *pbpG* gene, *pbpG* forward (5′-TTCTTCCTTTGTTGCCCGA CGTGGCAGCGAAAATGGTGGGAATTCGAGCTCTGCAGTCC-3′) and *pbpG* reverse (5′-AATAAACTGAGCATTCTTTTTCTCTATCCATCATGCT TGATAAGCTTGCATGCCTGCAG-3′). The primer pairs amplified the *res-npt-res* cassette and added sequences to its 5′ and 3′ ends that were identical to specific sites in the chromosome near the respective PBP genes. The near-*dacA* cassette was inserted approximately 1,300 bp from the *dacA* gene (replacing nucleotides 9207 to 9332 as described in the *E. coli* genome accession number AE000167) (Fig. 1A). The near-*dacB* cassette disrupted *yhbE*, the second open reading frame downstream from *dacB* (replacing nucleotides 3650 to 3739 of accession number AE000399) (Fig. 1B). The putative product of the *yhbE* gene encodes a hypothetical membrane protein of unknown function, but its closest homologues include amino acid-specific efflux pumps (data not shown). These mutants grew as well as wild type with no obvious phenotype. The near-*pbpG* cassette was inserted in a noncoding region between the *bglX* and *dld* genes (replacing nucleotides 7310 to 7331 of accession number AE000302) (Fig. 1C). Neither of these latter genes was disrupted, and neither the transcriptional terminator of *bglX* nor the promoter of *dld* was affected.

The amplified PCR products were transferred by electroporation into *E. coli* KM-32 (21), where they were incorporated into the chromosome via homologous recombination mediated by the phage lambda recombination system as described previously (18, 21, 22). Kanamycin-resistant colonies were selected, and colonies having the correct insertions were identified by diagnostic PCR of chromosomal DNA. The resulting strains were named BMKM16-1K (cassette insertion near *dacA*), KMAP-1K (insertion near *dacB*), and KMAP-3K (insertion near *pbpG*) (Fig. 1). P1 lysates were prepared on these strains and used to transduce *E. coli* CS109, creating strains BMCS16-1K (insertion near *dacA*), APCS-1 (insertion near *dacB*), and APCS-3 (insertion near *pbpG*). P1 lysates derived from these latter strains were used to transfer the wild-type *dacA*, *dacB*, or *pbpG* alleles to other PBP mutants.

FACS analysis. Strains containing no plasmids were incubated overnight in filtered T-soy broth (3 ml) in 13- by 100-mm tubes with shaking at 220 rpm in a gyratory water bath shaker (New Brunswick Scientific, New Brunswick, N.J.). Bacteria were diluted 1:250 into fresh T-soy broth and incubated with shaking until the absorbance at 600 nm (A_{600}) was 0.6. At this point, 1 ml was removed for staining and FACS analysis.

When testing to see if the morphological phenotypes of mutant strains could

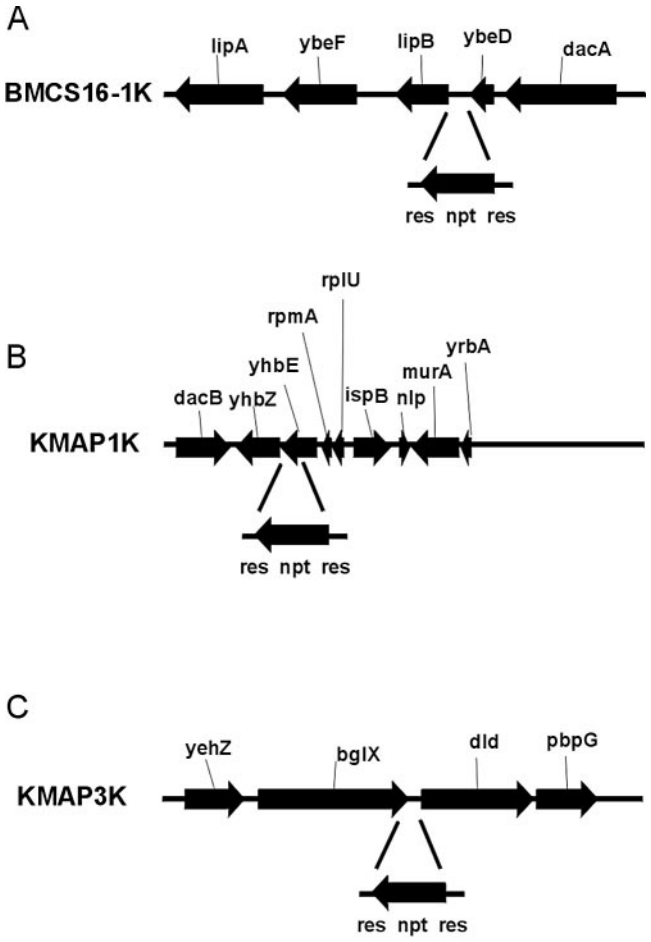

FIG. 1. Genomic location of the kanamycin resistance cassette (*res-npt-res*) near PBP genes. (A) Insertion near *dacA*, encoding PBP 5; (B) insertion near *dacB*, encoding PBP 4; (C) insertion near *pbpG*, encoding PBP 7. Strain names are given to the left of each map.

be complemented by cloned PBPs expressed from a plasmid, cultures were incubated overnight in filtered T-soy broth containing 20 μg of chloramphenicol/ml and 0.2% glucose to repress expression of the gene cloned under control of the arabinose promoter of pBAD18 (11). These overnight cultures were diluted three times: once early on the first morning, once late that evening, and a third time on the morning of the second day. Each dilution was 1:250 into fresh T-Soy broth containing 20 μg of chloramphenicol/ml but no glucose, so that cloned PBPs were expressed at a low level from the plasmid over a period of approximately 30 h. This procedure was designed to allow sufficient time for wild-type PBPs to be expressed and have time to complement any morphological defects, if possible. After the third dilution, cultures were incubated with shaking until the A_{600} reached 0.6, and 1 ml was removed for staining and FACS analysis.

For FACS analysis, cells were stained by adding 1 μl of the fluorescent dye SYTO BC (Molecular Probes, Eugene, Oreg.) to 1 ml of bacterial culture in T-soy medium, and the mixture was incubated in the dark at room temperature for 15 min. Afterwards, cells were fixed by adding neutral buffered formalin to a 1% final concentration. Samples were diluted 1:80 into FACSFlow buffer (catalog no. 340398; Becton Dickinson, Franklin Lakes, N.J.) and stored in the dark at room temperature until analysis, which was performed on the same day.

Fixed and stained cells were analyzed by using a FACSCalibur machine (Becton Dickinson), and the results were analyzed with CELLQUEST software, version 3.1f (Becton Dickinson). A standardized set of unstained beads (diameters of 0.21, 0.78, 2.60, 3.69, and 5.70 μm; Bangs Laboratories, Fishers, Ind.) was used to adjust the detectors so that the bacterial population was visible at the center of the detection screen. Detector voltages were adjusted until distinct populations, representing the differently sized beads, were observed. This procedure gave the following settings: forward scatter, E01; side scatter, 474 V; fluorescence (FL1), 396 V. These settings were used for all subsequent samples. The fluorescence channels were calibrated with Calbrite beads (Becton Dickinson Immunocytometry Systems) before each set of analyses. The threshold for a countable cell (primary detection parameter) was set to an FL1 of 52, to avoid counting nonstained inanimate background particles derived from lysed cells. For each sample, data from 20,000 cells were collected.

To compare cell populations with one another, the data for each strain were plotted on a two-dimensional graph (*x* axis, forward scatter; *y* axis, side scatter). As a control to which all other measurements could be compared, contour plots generated by the software were superimposed on the data set of the parental strain, *E. coli* CS109. Each contour line enclosed a different percentage of the sample and represented, in effect, the third dimension of the graph. These data (number of events within a specified area of the graph) could also be visualized as the height on the *z*-axis of a three dimensional graph. However, it was easier to analyze and report strain-to-strain variation in tabular form, according to the percentage of data points contained within each contour line. For this purpose, the distribution of data points of CS109 was used as the standard to which all other results were compared. Five contour lines were selected and used as guides to create sample gates, in which the innermost gate (gate 1) represented the peak of the third dimension and the outermost gate (5) represented almost all data points. These standardized gates were positioned over the data of mutant strains, and the numbers of cells in each gate were determined and compared with the normal distribution for strain CS109.

The Kolmogorov-Smirnov statistical test was used to compare raw data produced by FACS analysis. Other statistical and graphical analyses were performed using SigmaPlot software (SSPS, Chicago, Ill.) and Microsoft Excel (Microsoft Inc., Redmond, Wash.).

Microscopy. Cells were visualized and photographed as described previously (24). Briefly, mid-logarithmic-phase cells were immobilized on microscope slides covered with a thin layer of 1% agarose and viewed with a Nikon EFD-3 microscope with a 100× oil immersion objective. Photographs were obtained with an attached SenSys charge-coupled device camera and capture software (Photometrics Ltd., Tucson, Ariz.) at 1,000× total magnification.

RESULTS

Use of FACS to quantify shape differences. We chose FACS as a quantitative assay to replace the qualitative and visual microscopic evaluation of cell shape. Bacteria were stained with the fluorescent dye SYTO BC, which binds to total nucleic acid to produce a uniform fluorescence throughout live cells, and the light-scattering characteristics of labeled cells were measured by FACS. By plotting the forward- and side-scattered light from 20,000 fluorescent cells, the population of the parental strain CS109 clustered in a symmetrical peak on a three-dimensional graph (Fig. 2A) or in a two-dimensional scatter plot of the same data (Fig. 2B). However, the printed density of the scatter plots does not reflect the actual density of data points. To visualize this more accurately, the distribution of data in the scatter plot was represented by a series of contour lines generated by the FACS software (Fig. 2C). Each line encloses a different percentage of data points, and the set of lines is a topographical map representing different heights on the three-dimensional plot. Thus, the innermost contour line corresponds most closely to the position of the crest of the peak, and the outermost line encompasses greater than 99% of the total sample. In all cases we examined, and for unknown reasons, the amount of side scatter changed very little among mutants having different shapes (data not shown). Therefore, differences in cell shape were visualized most easily by graphing only the distribution of forward-scattered light (Fig. 2D).

To determine the reproducibility of morphological measurements by FACS, we assessed multiple independent samples of CS109 cells over a period of 6 months. For comparison purposes, a set of contour lines was derived from one of these samples to create five counting gates. These gates were super-

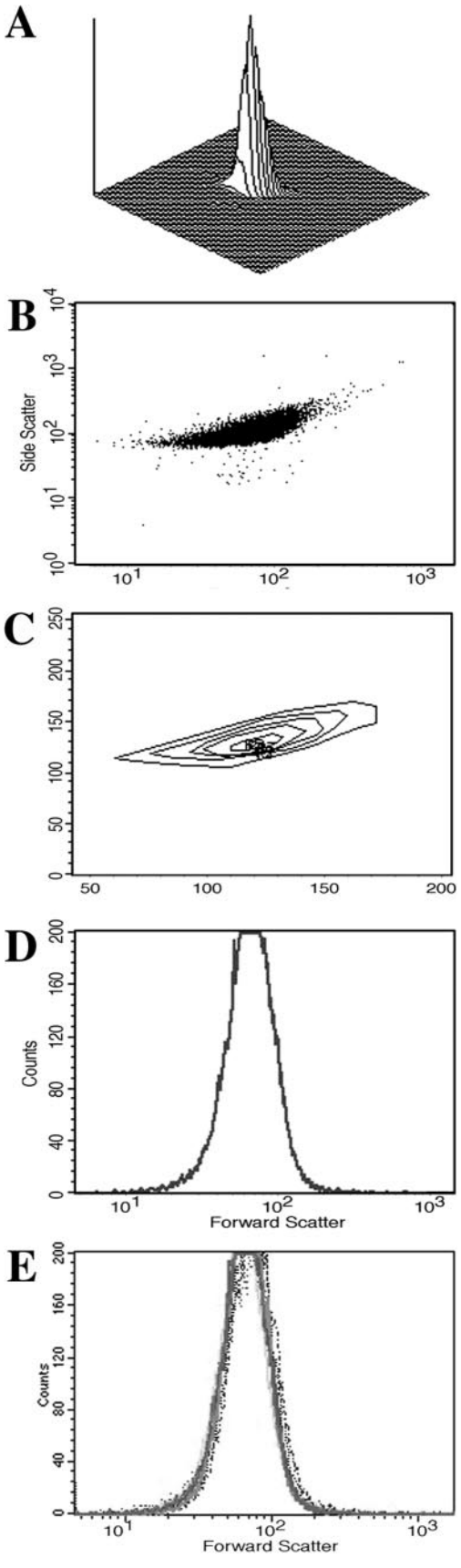

TABLE 2. FACS analysis of parental strain *E. coli* CS109

Sample[a]	Distribution of cells (%) within FACS gate[b]:				
	1	2	3	4	5
1	29.2	70.4	79.2	93.8	99.2
2	28.5	74.1	86.5	97.5	99.1
3	44.0	87.1	94.9	99.1	99.6
4	37.7	82.5	90.4	97.3	99.6
5	34.8	76.9	88.0	95.4	99.1
6	32.8	72.0	81.2	90.9	95.8
7	42.4	85.9	94.2	98.9	99.6
8	31.4	72.6	84.0	93.1	98.3
9	26.0	60.7	73.8	88.9	97.1
10	36.9	82.0	90.5	98.1	99.6
11	34.0	70.8	80.9	91.8	98.1
12	36.8	80.6	90.8	96.9	99.6
13	43.2	85.7	93.8	98.2	99.5
Avg ± SD	35.2 ± 5.7	77.0 ± 7.8	86.8 ± 6.5	95.4 ± 3.4	98.8 ± 1.2
Deviation (%)	16.2	10.1	7.5	3.6	1.2

[a] Independent experiments with cells grown on different days over a period of 6 months.

[b] FACS gates were drawn around a single CS109 population and superimposed on all other samples to give a relative comparison of cell distribution among gates.

imposed over each subsequent data set to determine the percentage of cells falling within each contour. Small variations in the position of the crest of each peak appeared as differences in the percentages of cells falling within the innermost gate, gate 1, whereas major movements of the entire sample population corresponded to different numbers of cells in gates 4 and 5 (Table 2). As expected, during repeated sampling of CS109 the amount of variation was greatest in gate 1 (±16% [standard deviation]), where minor differences in crest location would have the most pronounced effect. Variation became progressively smaller with increasing gate size, decreasing to ±3.6% and ±1.2% in gates 4 and 5, respectively (Table 2). The different forward scatter measurements for 13 repetitions were plotted against the benchmark CS109 results and showed a highly reproducible overlap of sample distributions (Fig. 2E). The Kolmogorov-Smirnov statistical test indicated these data were indistinguishable (data not shown). Similar reproducibility was observed for multiple samples of other strains (Table 3 and data not shown). Thus, FACS evaluation proved to be a reliable and reproducible way to quantify the general dimensions of a bacterial population.

To verify that FACS could detect morphological differences between strains, we compared the shape distributions of *E. coli* CS109 versus CS315-1 and CS345-3, two triple mutants previously shown to exhibit significant visual deformities (23). As

FIG. 2. FACS analysis of *E. coli* CS109. Cells were stained and analyzed by FACS as described in Materials and Methods. (A) Three-dimensional representation of the numbers of cells (*z* axis) with specific sizes and shapes denoted by forward-scattered light (*x* axis) and side-scattered light (*y* axis). (B) Dot plot of cells by forward-scattered (*x* axis) and side-scattered (*y* axis) light. (C) Contour plot representing the densities of the cell numbers in panel B. The fractions of the cell population from the innermost to the outermost rings are 35, 77, 89, 95, and 99%. (D) Numbers of CS109 cells (*y* axis) plotted according to the amount of forward-scattered light (*x* axis). (E) Thirteen superimposed FACS measurements of different CS109 cultures plotted as in panel D. The data are derived from the samples listed in Table 2.

TABLE 3. Cell shape distributions of PBP mutants

Strain[a]	PBP(s) deleted[b]	n[c]	Distribution of cells (%) within FACS gate[d]:		
			1	2	4
CS109	None	13	**35.2 ± 5.7**	**77.0 ± 7.8**	**95.4 ± 3.4**
BMCS04-1K	1a	4	27.1 ± 8.2	72.0 ± 9.5	96.0 ± 2.5
16-1	1b	4	19.4 ± 7.1	58.7 ± 8.5	89.2 ± 3.8
11-3	4	2	32.5 ± 6.7	74.3 ± 11	94.2 ± 5.1
12-7	5	6	**13.0 ± 1.2**	**38.0 ± 3.4**	**71.8 ± 4.8**
17-1	6	2	30.8 ± 5.8	71.2 ± 8.7	92.1 ± 4.4
9-19	7	2	30.5 ± 3.8	73.3 ± 6.3	94.5 ± 3.3
18-3	D	1	31.9	73.5	95.5
14-5	C	2	30.3 ± 2.8	71.8 ± 3.7	95.1 ± 0.9
15-3	H	2	33.2 ± 5.8	75.5 ± 8.4	95.6 ± 2.8
BMCS05-1K	1c	1	33.2	73.3	93.7
219-1	5, 4	3	11.2 ± 0.9	34.8 ± 3.0	67.0 ± 4.0
211-2	5, 6	1	11.3	35.0	69.1
204-1	5, 7	3	**9.4 ± 0.8**	**29.2 ± 1.4**	**62.0 ± 1.8**
235-1K	5, D	3	14.1 ± 0.7	40.1 ± 2.1	73.8 ± 1.6
216-2	5, C	1	12.1	37.5	72.5
215-3	5, H	1	11.9	36.3	70.1
232-1K	5, 1a	1	12.5	37.3	66.7
224-2	5, 1b	1	30.3	72.4	94.6
203-1B	4, 7	4	31.7 ± 10	70.1 ± 15	91.0 ± 6.9
205-1	6, 7	3	26.7 ± 1.9	64.4 ± 3.9	89.3 ± 4.4
206-3	7, H	3	35.6 ± 2.5	77.6 ± 2.9	95.8 ± 1.6
207-2	7, C	1	30.1	70.4	92.4
212-3	6, H	3	36.1 ± 3.2	78.2 ± 4.6	96.0 ± 2.4
213-1	6, C	1	31.3	72.3	93.4
221-3	4, H	1	40.5	85.4	97.8
222-1	4, C	1	33.1	75.3	95.4
236-1K	4, D	2	33.2 ± 4.0	70.4 ± 1.2	90.8 ± 3.6
237-1K	7, D	4	38.6 ± 2.0	82.0 ± 2.3	97.0 ± 1.3
322-1	5, 4, 6	3	13.0 ± 1.9	37.2 ± 6.6	70.4 ± 8.5
315-1	5, 4, 7	4	**6.8 ± 0.8**	**21.5 ± 2.5**	**54.5 ± 5.1**
326-3	5, 4, H	2	12.1 ± 3.1	34.1 ± 7.8	67.9 ± 10
331-1	5, 6, 7	2	10.1 ± 0.6	31.9 ± 1.0	70.6 ± 1.1
337-1	5, 6, C	2	11.0 ± 2.1	31.1 ± 5.6	62.6 ± 7.3
336-3	5, 6, H	2	11.2 ± 2.9	32.5 ± 7.6	64.7 ± 11
345-3	5, 7, H	4	**7.9 ± 0.8**	**23.7 ± 1.0**	**58.3 ± 1.2**
346-1	5, 7, C	2	10.4 ± 1.3	29.9 ± 3.1	64.2 ± 4.9
349-1	5, C, H	2	12.3 ± 4.8	33.3 ± 12	66.0 ± 14
371-1	5, 7, D	4	12.1 ± 6.7	32.7 ± 15	65.3 ± 13
373-1	5, 4, D	2	**6.1 ± 0.3**	**19.3 ± 1.1**	**51.8 ± 2.0**
395-1K	5, 6, D	2	**6.7 ± 0.2**	**20.3 ± 0.2**	**48.3 ± 0.2**
396-1K	5, D, C	2	15.7 ± 1.7	45.2 ± 3.6	79.3 ± 1.4
372-1	6, 7, D	3	17.4 ± 7.6	46.1 ± 17	77.3 ± 12
316-1	4, 6, 7	2	21.1 ± 0.5	54.3 ± 1.0	82.5 ± 0.5
318-1	4, 7, C	2	26.2 ± 2.7	65.0 ± 7.1	90.2 ± 4.7
387-1K	4, 7, D	2	26.6 ± 2.8	63.1 ± 4.5	87.9 ± 4.4
320-1	4, C, H	2	25.7 ± 5.8	62.1 ± 11	88.2 ± 7.0
388-1K	4, C, D	2	34.4 ± 0.2	77.7 ± 1.6	95.8 ± 0.9
389-1K	4, H, D	2	42.5 ± 1.5	86.7 ± 1.4	98.6 ± 0.0
323-3	4, 6, H	2	22.1 ± 0.3	57.2 ± 1.7	86.2 ± 0.1
343-1	6, 7, C	2	23.8 ± 2.3	59.8 ± 6.2	88.2 ± 3.3
332-3	6, 7, H	4	20.8 ± 5.1	53.6 ± 9.8	83.5 ± 7.0
334-1	6, C, H	2	23.1 ± 1.4	59.0 ± 5.2	86.7 ± 3.2
390-1K	6, C, D	2	29.4 ± 2.7	69.0 ± 4.9	93.0 ± 1.7
391-1K	6, H, D	2	35.6 ± 2.8	80.4 ± 3.7	96.5 ± 1.5
392-1K	7, C, D	2	30.4 ± 3.0	65.4 ± 1.3	89.5 ± 1.7
342-1	7, C, H	2	23.4 ± 9.0	57.1 ± 20	84.5 ± 14
393-1K	7, H, D	2	32.4 ± 2.0	84.6 ± 17	94.8 ± 2.7
394-1K	C, H, D	2	33.3 ± 0.5	71.2 ± 1.2	92.2 ± 1.6

[a] All strains were derived from *E. coli* CS109. Strain names with no alphabetical prefix are CS strains and have been described previously (4, 18, 23).
[b] Numbers refer to the respective PBPs (e.g., 1a = PBP 1a). D, DacD; C, AmpC; H, AmpH.
[c] Number of independent experiments.
[d] Gates were determined as described for Table 2. Numbers refer to the fraction of the population that falls within the respective gate (average percentage ± standard deviation). Values in bold highlight the results for the wild-type strain (CS109) plus the results of mutants that exhibited distributions especially different from that of the wild type, and these results are discussed in the text.

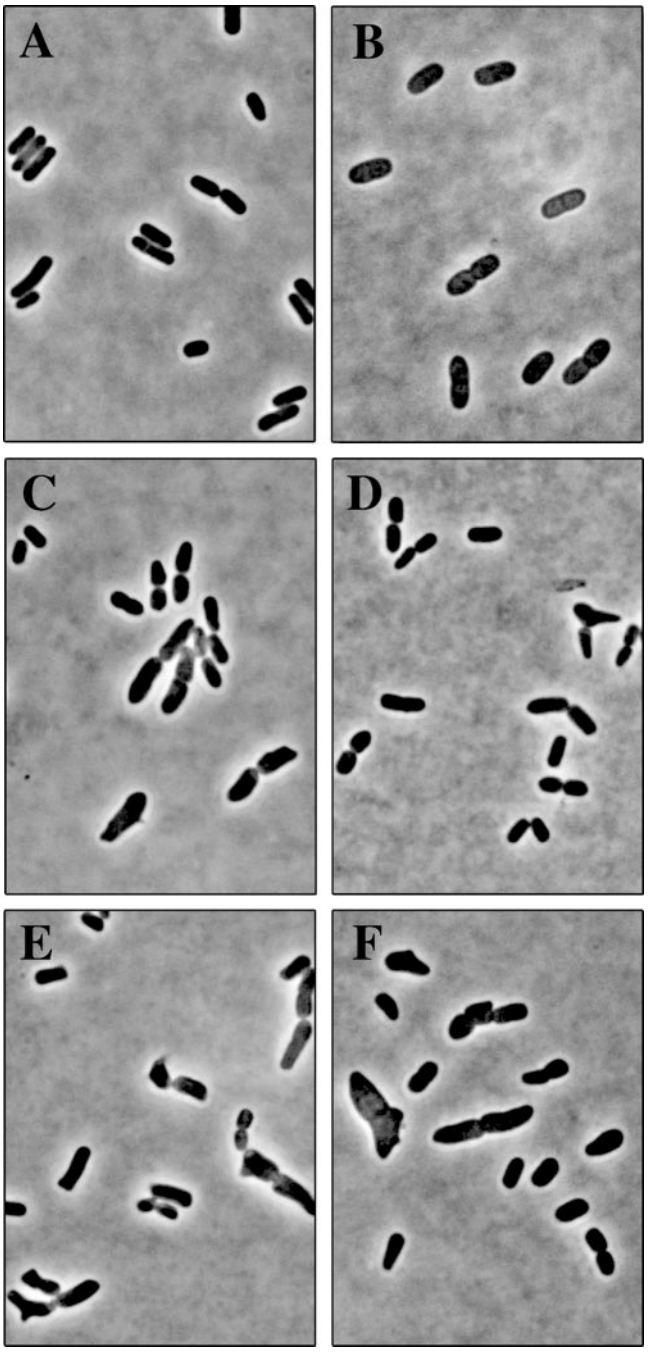

FIG. 3. Morphological effects of deleting PBPs from *E. coli*. Strains were grown to mid-log phase in LB (A) or T-soy broth (B to F) and affixed to agarose-coated slides for microscopy. All photographs are at the same magnification, with the newly divided cells in panel A being approximately 1.8 by 0.8 μm. (A and B) Parental strain CS109; (C and D) CS12-7 (ΔPBP 5); (E) CS315-1 (ΔPBPs 4, 5, and 7); (F) CS345-3 (ΔPBPs 5 and 7 and ΔAmpH).

expected, obvious shape aberrations were present in mutant cells (Fig. 3E and F) but not in the parent (Fig. 3B). When the strains were subjected to FACS analysis, three-dimensional plots (Fig. 4A and B) and forward-scatter graphs (Fig. 4C and D) revealed large differences in the distributions of sizes and shapes of cells from mutants compared to the parent. The mutant distributions were significantly different from CS109 ($P < 0.001$). As a means of quantifying the extent of these differences, we superimposed onto the mutant data five gated contours derived from CS109. The gates served as a stationary reference point from which we could compare how the distribution of cell shapes differed from that of the parent strain. As visualized by graphing forward scatter versus side scatter, it was clear that the distribution of mutant cell shapes moved away from the position of the parental contour lines (Fig. 4E and data not shown). The extent of the difference was even more clear after quantifying the numbers of cells in these gates. The percentages of cells distributed among the gates for CS315-1 and for CS345-3 were significantly different from the distribution exhibited by CS109 (Table 3). Therefore, the FACS procedure successfully detected and quantified the extent of shape differences among strains with known morphological differences.

Shape differences among PBP mutants. We were now in a position to quantify shape differences among a variety of PBP mutants. Each strain was grown to mid-logarithmic phase, harvested, and subjected to FACS analysis, and the data were tabulated to compare the distribution of cell shapes with the gated distribution of the parent strain (Table 3). Among the strains, the numbers of cells in all gates changed in the same direction, and so the results for only three gates are included in Table 3. Changes in gate 1 numbers indicated movement of the crest of the sample peak, and numerical changes in gates 2 and 4 indicated how far the bulk of the sample moved away from the control distribution.

The first surprise was that for CS12-7, the single Δ*dacA* mutant lacking only PBP 5, the shape distribution was clearly different from that of wild-type strain CS109 (Fig. 5A; Table 3), indicating that deleting PBP 5 by itself altered the shape of *E. coli*. No other mutant lacking only one PBP showed a similar change in shape (Fig. 5B and Table 3, strains BMCS04-1K to BMCS05-1K). This result was unexpected, because previous observations did not ascertain a shape change in CS12-7 by visual assay (23). However, in a retrospective inspection of photographs of the two strains, it was clear that many CS12-7 cells exhibited slight abnormalities at their poles (23) (data not shown). Also, slight deformities were visible in cells grown in T-soy medium in preparation for the FACS analysis (Fig. 3C and D), although it was difficult to assess the extent of these alterations. Thus, for this single PBP mutation, FACS analysis was able to measure and quantify shape defects that our group was previously unable or unwilling to credit by visual inspection alone.

Although the Δ*dacA* mutant was most different from the parent strain, a mutant lacking PBP 1b also exhibited a slightly different cell distribution (Fig. 5C and Table 3, strain 16-1). The differences were smaller than those exhibited by the Δ*dacA* strain and were confined primarily to gates 1 and 2. In addition, the population shift away from the wild-type distribution was opposite that observed for all other deformed cells (note the slight leftward shift in Fig. 5C). By time-lapse microscopy, we have observed that a small, random subset of ΔPBP1b mutant cells bloat and lyse during log-phase growth (B. Meberg, unpublished observations). The presence of this transient subpopulation of cells on their way to lysis probably

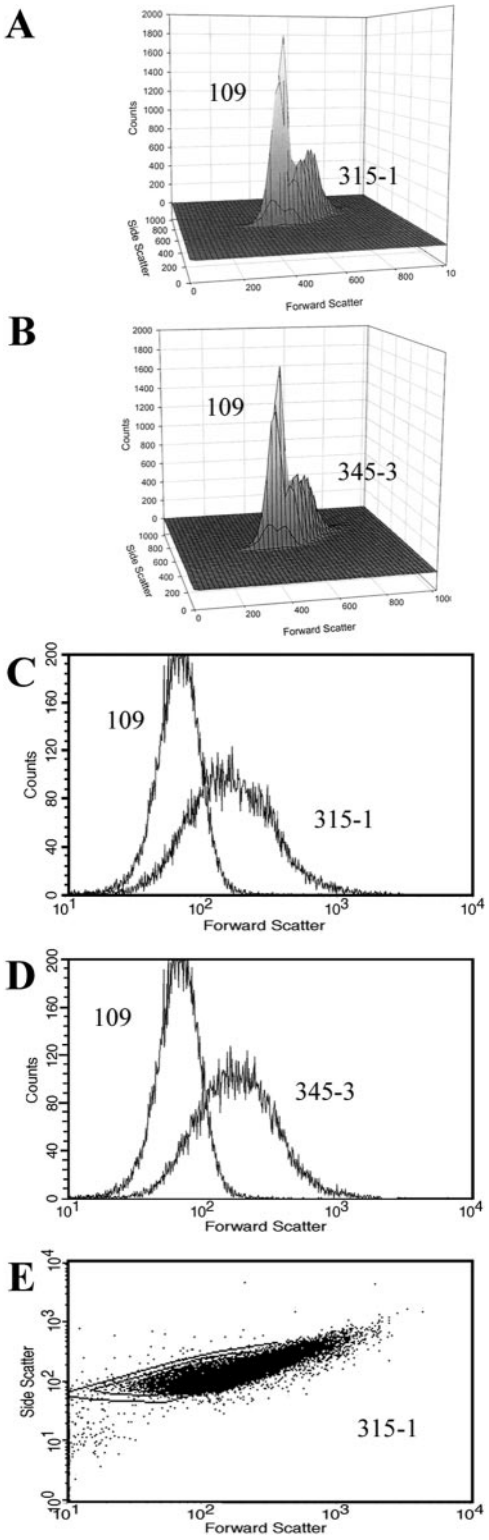

FIG. 4. Cell shape deficiencies detected by FACS analysis. The parental *E. coli* strain (109) and mutants lacking PBPs 4, 5, and 7 (315-1) or PBPs 5 and 7 and AmpH (345-3) were stained and analyzed by FACS. (A and B) Three-dimensional comparisons of the population distributions of the parental strain (left peak) and the mutant strain (right peak). (C and D) Comparison of the population distributions of the parental strain and mutants by using only forward-scattered light (*x* axis). (E) Dot plot of the FACS distribution of forward-scattered light (*x* axis) versus side-scattered light (*y* axis) for cells of CS315-1 as superimposed on the contour lines derived from the FACS distribution of the parental strain, CS109. The distribution of mutant strain values is shifted to the right relative to that of the CS109 contours.

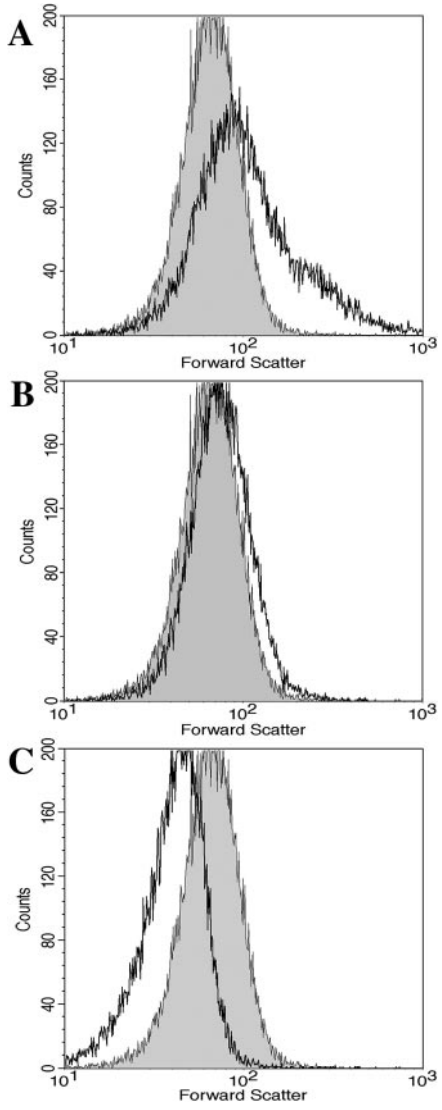

FIG. 5. Cell shape deficiencies of *E. coli* mutants lacking single PBPs. The parental *E. coli* strain CS109 (gray-filled peaks) and mutants lacking single PBPs (dark lines without fill) were stained and analyzed by FACS. (A) CS109 versus CS12-7 (ΔPBP5). (B) CS109 versus CS17-1 (ΔPBP6). Note that strains lacking any one of PBPs 4, 6, and 7, DacD, AmpC, or AmpH all gave identical overlapping FACS population curves. (C) CS109 versus CS16-1 (ΔPBP1b).

skews the distribution of particles in PBP 1b mutants. Since visual inspection confirmed that virtually all viable cells in this mutant had normal shapes (data not shown), differences in FACS distribution in PBP 1b mutants probably reflect this prelysis phenomenon instead of shape alterations.

The effect on cell shape carried over into double mutants from which PBP 5 and a second PBP were deleted (Table 3, strains 219–1 to 232-1K). In every case, shape distribution

TABLE 4. Effect of gene replacements on cell shape distributions in PBP mutants

Strain[a]	PBPs deleted[b]	PBP replaced[b]	n[c]	Distribution of cells (%) within FACS gate[d]:		
				1	2	4
109 (parent)	None		13	35.2 ± 5.7	77.0 ± 7.8	95.4 ± 3.4
315-1	4, 5, 7		4	6.8 ± 0.8	21.5 ± 2.5	54.5 ± 5.1
APCS204-1	5, 7	4	2	11.2 ± 0.3	35.1 ± 0.5	69.6 ± 1.4
204-1	5, 7		3	9.4 ± 0.8	29.2 ± 1.4	62.0 ± 1.8
APCS219-1	4, 5	7	2	11.2 ± 0.7	34.0 ± 1.5	66.1 ± 2.6
219-1	4, 5		3	11.2 ± 0.9	34.8 ± 3.0	67.0 ± 4.0
BMCS203-1B	4, 7	5	3	38.9 ± 6.7	81.5 ± 9.7	96.2 ± 4.2
203-1B	4, 7		4	31.7 ± 10	70.1 ± 15	91.0 ± 6.9

[a] All strains were derived from *E. coli* CS109. Strain names with no alphabetical prefix are CS strains and have been described previously (4, 18, 23).
[b] Numbers refer to the respective PBPs. "PBP replaced" denotes that the wild-type version of the indicated PBP replaced genes originally deleted from CS315-1.
[c] Number of independent experiments.
[d] Gates were determined as described for Tables 2 and 3.

deviated significantly from normal. Once again, this was contrary to our previous reports derived from microscopy alone (23). The degree to which these double mutants departed from the normal shape distribution depended on the second missing PBP. Mutants combining a PBP 5 deletion with a deletion of PBP 4, PBP 6, DacD, AmpC, AmpH, or PBP 1a were no more deviant than was the CS12-7 strain lacking only PBP 5 (Table 3, 219-1, 211-2, and 235-1K to 215-3). On the other hand, the double mutant missing PBPs 5 and 7 (CS204-1) was consistently more abnormal than the mutant lacking only PBP 5 (Table 3, strain 12-7), indicating that losing PBP 7 had an additive effect on cell shape. Note that double mutants lacking PBPs other than PBP 5 retained normal cell shape distributions (Table 3, strains 203-1B to 237-1K), underscoring the primary importance of PBP 5 for this phenotype.

The double mutant lacking PBPs 1b and 5 provided a curious exception to the rule that all PBP 5 mutants were misshapen (Table 3, strain 224–2). In this case, the distribution of cell shapes was indistinguishable from that of the CS109 parent (Table 3). The answer appears to lie in the rapid lysis of misshapen cells in this double mutant. Time-lapse microscopy of microcolonies revealed that malformed cells lysed extremely rapidly once they appeared (B. Meberg, unpublished). Because the remaining cells appeared morphologically normal, FACS analysis detected a wild-type distribution of cell shapes.

Previously, our group showed that the most dramatic visual morphological deficiencies in *E. coli* required that the cells be missing PBP 5 and at least two additional LMW PBPs (23). FACS analysis confirmed and quantified these visual results. In particular, the most misshapen triple mutants were CS315-1 (ΔPBPs 4, 5, and 7), CS373-1 (ΔPBPs 4 and 5 and DacD), and CS395-1K (ΔPBPs 5 and 6 and DacD) (Table 3). Each of these mutants exhibited a distribution of misshapen cells greater than that exhibited by the single PBP 5 mutant (Table 3, strain 12-7), the double mutant missing PBPs 5 and 7 (Table 3, strain 204-1), or any other triple mutant. This indicates that deletion of particular PBPs accentuates morphological abnormalities when PBP 5 is missing. Specifically, deletion of PBPs 4 and 7 (strain CS315-1) produced a morphological effect clearly worse than that produced by deleting either protein in the absence of PBP 5 (Table 3 and Fig. 3E), suggesting that these two endopeptidases have at least partially overlapping functions. The behavior of other strains implies that DacD (CS373-1) and PBP 6 (CS395-1K) may also influence cell shape when combined in specific genetic backgrounds (Table 3).

The results highlight the primary role of PBP 5 in shape determination. Particularly noteworthy is the observation that the double mutant lacking PBPs 4 and 7 (CS203-1B) exhibits a shape distribution equivalent to that of the parental strain CS109 (Table 3). In addition, this double mutant is no different from strains lacking only PBP 4 (Table 3, strain 11-3) or PBP 7 (Table 3, strain 9-19). Thus, the shape contribution of PBPs 4 and 7 is observed only when PBP 5 is absent. Other triple mutants that retained a wild-type PBP 5 also produced normal or near-normal shape distributions (Table 3, strains 316-1 to 394-1K). However, in a few cases the cell shape distributions were slightly skewed even in the presence of active PBP 5, suggesting the intriguing possibility that small morphological effects may be produced by deleting other PBPs, an observation we could not make by visual inspection. We have been unable to assess the morphological bases of these changes because the deviations from wild type were so minor.

Reversal of shape abnormalities by gene replacement. To further test the idea that PBPs 4 and 7 were active in the morphological pathway, we reinserted wild-type PBP genes into the chromosome of *E. coli* CS315-1 (ΔPBPs 4, 5, and 7). If adding back wild-type versions of PBPs 4, 5, or 7 could reverse the defects of this triple mutant, then the gated cell distributions should return to those exhibited by double mutants. In fact, such chromosomal replacements did return the shape distributions to those of the analogous double mutants (Table 4). For example, when wild-type PBP 4 was moved back into the chromosome of CS315-1 to create APCS204-1 (Table 4), the distribution of misshapen cells became more normal than that of CS315-1 and more like that of CS204-1, the mutant lacking PBPs 5 and 7 (Table 4). Reinserting wild-type PBP 7 resulted in a strain (Table 4, APCS219-1) that had an essentially identical cell distribution as the original double mutant, CS219-1 (Table 4). Also, as expected, replacing wild-type PBP 5 in CS315-1 (Table 4, strain BMCS201-1B) returned the strain to a shape distribution indistinguishable from that of the parent CS109 or CS203-1B, the mutant lacking PBPs 4 and 7 (Table 4).

We also complemented strains CS315-1 (ΔPBPs 4, 5, and 7), CS345-3 (ΔPBPs 5 and 7 and Δ*ampH*), and CS373-1 (ΔPBPs 4 and 5 and Δ*dacD*) by transforming the mutants with pBAD18-

Cm-derived plasmids carrying individual wild-type PBPs. By visual inspection, PBPs 4, 5, and 7 reduced the frequency and extent of shape deformities, but complementation with PBP 6, DacD, or AmpH did not (data not shown). Overall, the results confirmed that PBPs 4 and 7 contributed to maintenance of uniform shape in cells lacking PBP 5.

Effect of growth medium on development of abnormalities. We wondered why FACS analysis detected morphological effects in single and double PBP mutants when we had reported no significant visual effects previously. First, it is likely the alterations were so slight we had dismissed them as insignificant. In fact, as mentioned above, when we looked more closely at a strain lacking only PBP 5 we could identify minor imperfections (Fig. 3C and D) that were not present in the parent strain (Fig. 3A and B). A second contributing factor might have been a difference in the way cells were grown prior to the FACS procedure. Strains destined for FACS analysis were incubated in T-soy broth instead of LB, because the SYTO-BC staining procedure called for a low-phosphate medium. Indeed, the morphology of the parental strain CS109 was altered by growth in T-soy medium (Fig. 3A versus B). Cells incubated in T-soy were slightly wider than those grown in LB, and mutants lacking multiple PBPs exhibited more pronounced shape alterations than did cells incubated in LB broth (Fig. 3 and data not shown). We do not know how this growth effect enhanced or accentuated the morphological imperfections, but the phenomenon depended on an unidentified substance in the yeast extract component of LB (data not shown).

DISCUSSION

Because the LMW PBPs are not essential for bacterial growth in the laboratory, their physiological functions have remained mysterious for three decades. This is odd, because the enzymes are widely distributed—most bacteria have six to eight LMW PBPs, though some gram-positive cocci express only one (20, 27)—and their ubiquity implies they have an important purpose in growth or survival. Previously, our group discovered that deleting PBP 5 plus at least two additional LMW PBPs had a dramatic effect on cell shape in *E. coli* (23, 24). However, it is now clear that our original visual microscopic assay was insensitive to minor shape changes. FACS analysis circumvented this problem and detected slight morphological alterations in mutants lacking only PBP 5, reinforcing the impression that this protein plays a central role in shape determination. The fact that shape abnormalities were exacerbated by deleting PBPs 4 and 7 from a PBP 5 mutant indicates these two endopeptidases are accessory enzymes that moderate cell shape.

How might the LMW PBPs influence cell shape? The major biochemical activities of PBPs 4, 5, and 7 are illustrated in Fig. 6 (16, 17). PBP 5 is a DD-carboxypeptidase that removes the terminal D-alanine residue from the short peptide side chain that extends from each *N*-acetylmuramic acid moiety of the oligomeric glycan backbone (Fig. 6, compound A to compound B). PBPs 4 and 7 are endopeptidases that cleave cross-linked side chains previously linked by one or more of the high-molecular-weight PBPs during peptidoglycan synthesis (Fig. 6, compound C to compound B). Thus, in the absence of PBP 5,

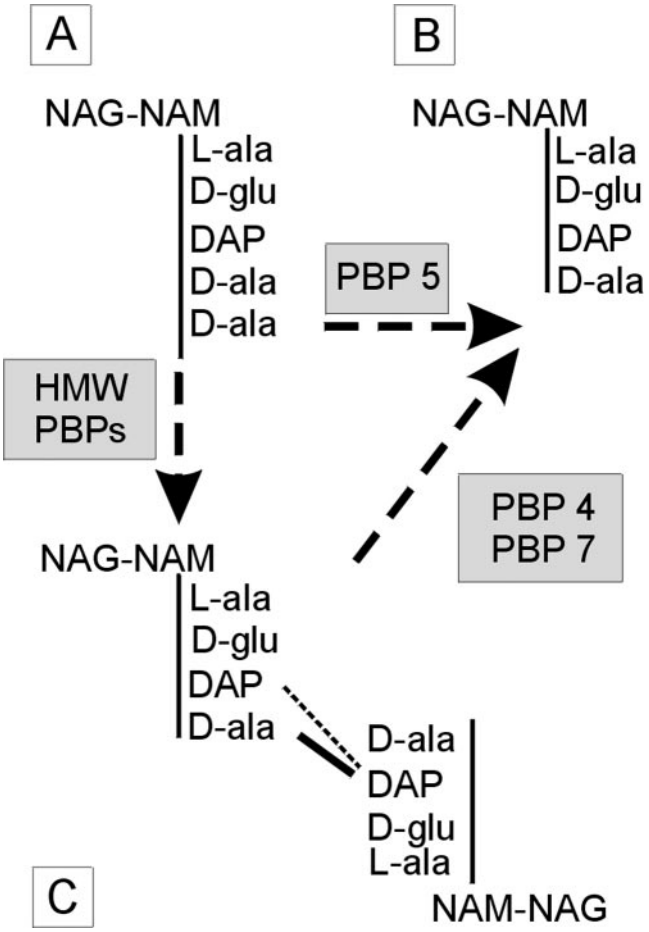

FIG. 6. Activities of different PBPs on peptidoglycan subunits. The high-molecular-weight PBPs (HMW PBPs) polymerize monomeric subunits into glycan chains, some of which are also cross-linked via their peptide side chains. PBP 5 removes the terminal D-alanine from pentapeptide side chains, and PBPs 4 and 7 cleave cross-linked peptide side chains. (Note that PBP 6 and DacD might also act as DD-carboxypeptidases to give the same reactions as PBP 5. Also, the slight facility of PBP 4 as a DD-carboxypeptidase has been omitted from this scheme.) (A) Pentapeptide monomer; (B) tetrapeptide monomer; (C) cross-linked tetrapeptide subunits. The lines represent two possible linkages: a 4–4 linkage (solid line) and a 3–4 linkage (dotted line). D-glu, D-glutamic acid; L-ala, L-alanine; DAP, diaminopimelic acid; D-ala, D-alanine.

pentapeptide peptidoglycan subunits (muropeptides) such as compound A accumulate to higher than normal amounts (13). Because muropeptides with pentapeptide side chains are the only compounds that can act as donors in the cross-linking reaction, deleting PBP 5 increases the amount of these substrates available to yield form C. On the other hand, in the presence of PBPs 4 or 7, cross-linked subunits (compound C) are degraded to monomeric muropeptides (compound B). Thus, the amount of certain cross-linked products may increase in the absence of PBP 5, and their lifetimes may be prolonged in the absence of PBPs 4 and 7. The order of these reactions may also explain the relative importance of PBP 5 compared to other enzymes. In this scheme, PBP 5 activity determines the availability of cross-link-proficient substrates at an early stage in the pathway, whereas PBPs 4 and 7 act on the

cross-linked products themselves, which may be sequestered or otherwise unavailable for rapid degradation. For example, so far as is known, PBP 7 acts only on intact sacculi (28), which may impair the accessibility of PBP 7 to its substrates or limit the rate at which it can cleave cross-links. As for the nature of the cross-linked structures that accumulate, one attractive possibility is that they comprise metabolically inert peptidoglycan which is normally present only at cell poles but is correlated with deformed sites in shape-defective mutants (5, 6).

The present results underscore, again, that the physiological functions of PBP 5 are set apart from the other DD-carboxypeptidases in *E. coli*, PBP 6 and DacD. The three proteins are distinguished by subtle enzymatic differences arising from minor sequence variations at their active sites (10), and so they may act on different substrates or have different enzymatic activities. The most distinctive characteristic of PBP 6 is that it accumulates as cells enter stationary phase (2, 31), but the rationale for this is unknown. No physiological role has been described for DacD. The fact that most gram-negative bacteria carry multiple DD-carboxypeptidase homologues suggests these enzymes perform important functions, but what these may be remains highly speculative. We did observe slight morphological effects in the absence of PBP 6 and DacD in a few genetic backgrounds but, so far, the information is insufficient to include them in a reaction scheme with PBPs 4, 5, and 7.

What might these results say about the roles of the LMW PBPs in gram-positive bacteria? First of all, though *B. subtilis* encodes a large number of LMW PBPs, the loss of one or more does not adversely affect the cell shape of this organism (25, 26). And yet, *Staphylococcus aureus*, *Streptococcus pyogenes*, and *Streptococcus pneumoniae* each express only a single DD-carboxypeptidase, and the loss of this LMW PBP does have morphological consequences in these bacteria (12, 30). This implies the enzyme also plays a pivotal role in the coccoid bacteria.

Finally, recent results hint that the LMW PBPs may mediate their morphological effects by altering an FtsZ-dependent reaction during cell division. Morlot et al. observed that the DD-carboxypeptidase PBP 3 of *S. pneumoniae* influences the progression of cell division by disconnecting invagination of the FtsZ ring from the activity of peptidoglycan synthetic PBPs (20), suggesting that this LMW PBP regulates the linkage between peptidoglycan synthesis and septation. In addition, we observed that manipulating these two systems creates a curious morphological effect. Inhibiting FtsZ by expressing SulA or MinC in an *E. coli* strain lacking PBPs 5 and 7 forces a subpopulation of the resulting filaments to grow as left-handed helices, which therefore adopt spirillum-like forms (33). The data support the idea that certain LMW PBPs regulate an undefined interaction between peptidoglycan synthesis and FtsZ-driven division events. Such a connection between FtsZ and the activity of the LMW PBPs has been proposed on the basis of historical data (35). Overall, the results from several organisms suggest that the main biological function of the LMW PBPs may be to act as morphological switches, possibly by influencing the types of substrates available to different enzymes during cell division.

ACKNOWLEDGMENTS

We thank David Nelson and Anindya Ghosh for helpful discussions and Margaret Larson for laboratory assistance.

This work was supported by grant GM61019 from the National Institutes of Health.

REFERENCES

1. **Bianchi, M.** 1989. Unusual bloom of star-like prosthecate bacteria and filaments as a consequence of grazing pressure. Microb. Ecol. **17:**137–141.
2. **Buchanan, C. E., and M. O. Sowell.** 1982. Synthesis of penicillin-binding protein 6 by stationary phase *Escherichia coli.* J. Bacteriol. **151:**491–494.
3. **Daniel, R. A., and J. Errington.** 2003. Control of cell morphogenesis in bacteria. Two distinct ways to make a rod-shaped cell. Cell **113:**767–776.
4. **Denome, S. A., P. K. Elf, T. A. Henderson, D. E. Nelson, and K. D. Young.** 1999. *Escherichia coli* mutants lacking all possible combinations of eight penicillin binding proteins: viability, characteristics, and implications for peptidoglycan synthesis. J. Bacteriol. **181:**3981–3993.
5. **de Pedro, M. A., J. C. Quintela, J.-V. Höltje, and H. Schwarz.** 1997. Murein segregation in *Escherichia coli.* J. Bacteriol. **179:**2823–2834.
6. **de Pedro, M. A., K. D. Young, J.-V. Höltje, and H. Schwarz.** 2003. Branching of *Escherichia coli* cells arises from multiple sites of inert peptidoglycan. J. Bacteriol. **185:**1147–1152.
7. **Dusenbery, D. B.** 1998. Fitness landscapes for effects of shape on chemotaxis and other behaviors of bacteria. J. Bacteriol. **180:**5978–5983.
8. **Faulkner, G., and R. A. Garduño.** 2002. Ultrastructural analysis of differentiation in *Legionella pneumophila.* J. Bacteriol. **184:**7025–7041.
9. **Figge, R. M., A. V. Divakaruni, and J. W. Gober.** 2004. MreB, the cell shape-determining bacterial actin homologue, co-ordinates cell wall morphogenesis in *Caulobacter crescentus.* Mol. Microbiol. **51:**1321–1332.
10. **Ghosh, A. S., and K. D. Young.** 2003. Sequences near the active site in chimeric penicillin binding proteins 5 and 6 affect uniform morphology of *Escherichia coli.* J. Bacteriol. **185:**2178–2186.
11. **Guzman, L.-M., D. Belin, M. J. Carson, and J. Beckwith.** 1995. Tight regulation, modulation, and high-level expression by vectors containing the arabinose P_{BAD} promoter. J. Bacteriol. **177:**4121–4130.
12. **Henze, U. U., M. Roos, and B. Berger-Bächi.** 1996. Effects of penicillin-binding protein 4 overproduction in *Staphylococcus aureus.* Microb. Drug Resist. **2:**193–199.
13. **Kraus, W., and J.-V. Höltje.** 1987. Two distinct transpeptidation reactions during murein synthesis in *Escherichia coli.* J. Bacteriol. **169:**3099–3103.
14. **Kristensen, C. S., L. Eberl, J. M. Sanchez-Romero, M. Givskov, S. Molin, and V. de Lorenzo.** 1995. Site-specific deletions of chromosomally located DNA segments with the multimer resolution system of broad-host-range plasmid RP4. J. Bacteriol. **177:**52–58.
15. **Lutkenhaus, J., and S. G. Addinall.** 1997. Bacterial cell division and the Z ring. Annu. Rev. Biochem. **66:**93–116.
16. **Matsuhashi, M.** 1994. Utilization of lipid-precursors and the formation of peptidoglycan in the process of cell growth and division: membrane enzymes involved in the final steps of peptidoglycan synthesis and the mechanism of their regulation, p. 55–71. *In* J.-M. Ghuysen and R. Hakenbeck (ed.), Bacterial cell wall. Elsevier Science B.V., Amsterdam, The Netherlands.
17. **Matsuhashi, M., S. Tamaki, S. J. Curtis, and J. L. Strominger.** 1979. Mutational evidence for identity of penicillin-binding protein 5 in *Escherichia coli* with the major D-alanine carboxypeptidase IA activity. J. Bacteriol. **137:**644–647.
18. **Meberg, B. M., F. C. Sailer, D. E. Nelson, and K. D. Young.** 2001. Reconstruction of *Escherichia coli mrcA* (PBP 1a) mutants lacking multiple combinations of penicillin binding proteins. J. Bacteriol. **183:**6148–6149.
19. **Miller, J. H.** 1972. Experiments in molecular genetics. Cold Spring Harbor Laboratory, Cold Spring Harbor, N.Y.
20. **Morlot, C., M. Noirclerc-Savoye, A. Zapun, O. Dideberg, and T. Vernet.** 2004. The D,D-carboxypeptidase PBP3 organizes the division process of *Streptococcus pneumoniae.* Mol. Microbiol. **51:**1641–1648.
21. **Murphy, K. C.** 1998. Use of bacteriophage lambda recombination functions to promote gene replacement in *Escherichia coli.* J. Bacteriol. **180:**2063–2071.
22. **Murphy, K. C., K. G. Campellone, and A. R. Poteete.** 2000. PCR-mediated gene replacement in *Escherichia coli.* Gene **246:**321–330.
23. **Nelson, D. E., and K. D. Young.** 2001. Contributions of PBP 5 and DD-carboxypeptidase penicillin binding proteins to maintenance of cell shape in *Escherichia coli.* J. Bacteriol. **183:**3055–3064.
24. **Nelson, D. E., and K. D. Young.** 2000. Penicillin binding protein 5 affects cell diameter, contour, and morphology of *Escherichia coli.* J. Bacteriol. **182:**1714–1721.
25. **Popham, D. L., M. E. Gilmore, and P. Setlow.** 1999. Roles of low-molecular-weight penicillin-binding proteins in *Bacillus subtilis* spore peptidoglycan synthesis and spore properties. J. Bacteriol. **181:**126–132.
26. **Popham, D. L., and K. D. Young.** 2003. Role of penicillin-binding proteins in bacterial cell morphogenesis. Curr. Opin. Microbiol. **6:**594–599.
27. **Pucci, M. J., and T. J. Dougherty.** 2002. Direct quantitation of the numbers of individual penicillin-binding proteins per cell in *Staphylococcus aureus.* J. Bacteriol. **184:**588–591.
28. **Romeis, T., and J.-V. Höltje.** 1994. Penicillin-binding protein 7/8 of *Escherichia coli* is a DD-endopeptidase. Eur. J. Biochem. **224:**597–604.
29. **Sambrook, J., E. F. Fritsch, and T. Maniatis.** 1989. Molecular cloning: a

laboratory manual, 2nd ed. Cold Spring Harbor Laboratory Press, Cold Spring Harbor, N.Y.
30. **Schuster, C., B. Dobrinski, and R. Hakenbeck.** 1990. Unusual septum formation in *Streptococcus pneumoniae* mutants with an alteration in the D,D-carboxypeptidase penicillin-binding protein 3. J. Bacteriol. **172:**6499–6505.
31. **van der Linden, M. P., L. de Haan, M. A. Hoyer, and W. Keck.** 1992. Possible role of *Escherichia coli* penicillin-binding protein 6 in stabilization of stationary-phase peptidoglycan. J. Bacteriol. **174:**7572–7578.
32. **van Loosdrecht, M. C., W. Norde, and A. J. Zehnder.** 1990. Physical chemical description of bacterial adhesion. J. Biomater. Appl. **5:**91–106.
33. **Varma, A., and K. D. Young.** 2004. FtsZ collaborates with penicillin binding proteins to generate bacterial cell shape in *Escherichia coli.* J. Bacteriol. **186:**6768–6774.
34. **Weiss, T. H., A. L. Mills, G. M. Hornberger, and J. S. Herman.** 1995. Effect of bacterial cell shape on transport of bacteria in porous media. Environ. Sci. Technol. **29:**1737–1740.
35. **Young, K. D.** 2003. Bacterial shape. Mol. Microbiol. **49:**571–580.